Liquid-liquid dispersions in intensified impinging-jets cells

CrossMark

Dimitrios Tsaoulidis, Panagiota Angeli *

Department of Chemical Engineering, University College London, WC1E 7JE London, UK

HIGHLIGHTS

- Development of a novel impinging-jets contactor for immiscible liquids.
- Characterisation of drops sizes and interfacial areas for a wide range of conditions.
- Interfacial areas with the impinging-jets cell were up to two orders of magnitude larger than in conventional contactors.
- Sauter mean drop diameters in the contactor were correlated with the specific energy dissipation rate at the impinging zone.

ARTICLE INFO

ABSTRACT

The formation of dispersions of two immiscible liquids in a confined impinging-jets cell was studied experimentally. The jets of the liquids formed at two opposing channels and collided in a main channel, which was perpendicular to the previous two. Jet channels with diameters either 0.25 or 0.5 mm and main channels with diameters either 2 or 3 mm were used. The jet velocities varied from 0.17 to 6.2 m/s and the dispersed to continuous phase ratios varied from 0.05 to 0.28. Deionised water and kerosene (Exxsol D80: ρ = 795 kg/m^3 and μ = 1.73 mPa s) were used as test fluids. Drop sizes were measured with high-speed imaging. It was found that the total velocity of the two jets was the main parameter that affected both the average drop size and the interfacial area, whilst the dispersed to continuous phase flow rate ratio was less significant. Both phases could become continuous depending on the phase flowrate ratio; drops were, however, larger in the organic continuous dispersions. The interfacial area produced with the impinging-jets cell was almost 3 times larger than in capillary contactors at similar conditions (u_{mix} = 0.024–0.19 m/s). The size of the main channel affected the drop size and smaller drops formed in the large channel compared to the small one. With increasing energy dissipation rate, ε, in the impingement zone, the Sauter mean diameter decreased following a relation of the form $\sim\varepsilon^{-b}$. Apart from the lower velocities, the drop sizes did not change significantly at distances equal to 15 channel diameters downstream the impingement area.

© 2017 The Authors. Published by Elsevier Ltd. This is an open access article under the CC BY license (http://creativecommons.org/licenses/by/4.0/).

1. Introduction

Dispersed liquid-liquid flows find many applications in process, food and pharmaceutical industries, and wastewater treatment. Among others, dispersions are usually generated in stirred tanks, in-line mixers, or high-pressure homogenisers (Chen and Middleman, 1967; Das et al., 2013; Daub et al., 2013; Lee and Norton, 2013; Lemenand et al., 2003), where non-uniform flow fields often result in wide drop size distributions. Microfluidic devices have also been used for the generation of dispersions with narrow size distribution (Parhizkar et al., 2013). The flowrates possible with microfluidic devices are, however, small and limit their industrial application.

Narrow drop size distributions and high throughputs can be achieved in impinging-jets cell configurations, where two fluid streams collide with each other at high flow rates (Mahajan and Kirwan, 1996). The energy dissipation due to collision and redirection of the fluid jets in small volumes can be one to two orders of magnitude higher than in conventional contactors (Maaβ et al., 2011; Saien et al., 2006) and should result in small drop sizes and large interfacial areas. The formation of dispersions is influenced by the energy released during the collision of the opposing jets, while the uniformity of the dispersions depends on the geometric design, the phase ratio, and the intensity of mixing in the impingement zone (Siddiqui, 2014).

---

* Corresponding author.
  E-mail address: p.angeli@ucl.ac.uk (P. Angeli).

Nomenclature

Symbols

A	cross sectional area (m^2)
b	adjustable parameter
d_i	diameter of the indiviadual drop (mm)
d_j	nozzle internal diameter (mm)
D[1,0]	arithmetic mean diameter (mm)
D[3,2]	Sauter mean diameter (mm)
D_{max}	maximum drop size (mm)
D	main channel internal diameter (mm)
k	adjustable parameter
L	length of the channel (mm)
m_i	mass flowrate of phase i (kg/s)
n	number of drops
PdI	polydispersity index (–)
P_k	kinetic energy (J)
Q	flow rate (m^3/s)
r	phase ratio Q_d/Q_c (–)

Re	Reynolds number (–)
u_j	superficial velocity of the jet (m/s)
u_{mix}	superficial mixture velocity (m/s)
u_d	velocity of the drop (m/s)
V_{iz}	volume of the impingement zone (m^3)

Greek symbols

α	Interfacial area (m^2/m^3)
ρ	density (kg/m^3)
σ	standard deviation
φ	volume fraction of the dispersed phase (–)

Subscripts

c	continuous
d	dispersed
j	jet
mix	mixture

The collision of jet streams in a confined space has mainly been investigated for miscible liquid streams (Fonte et al., 2015; Gao et al., 2013; Icardi et al., 2011; Metzger and Kind, 2016). Sultan et al. (2012) studied with PLIF the collision of two liquid jets for different geometrical and operational parameters and found that a chaotic regime forms in the impingement zone. Mahajan and Kirwan (1996) characterized micro-mixing effects in an impinging-jets mixer by using a two-step Bourne reaction scheme between 1-napthol and diazosulfanilic acid. Moreover, Siddiqui et al. (2009) estimated that the energy dissipation rate in an impinging-jets reactor was almost 2 orders of magnitude higher than in stirred tanks. They also measured the micro-mixing efficiency for a homogeneous and a heterogeneous reaction over a wide range of mixing conditions and reported higher product yield compared to a CSTR reactor.

The studies on impinging jets with immiscible liquids in confined spaces are very limited and have mainly focused on the mass transfer performance of the devices, but not on the hydrodynamic characteristics. Jets were used for extraction separations involving an aqueous and an organic phase by Dehkordi (2001), but their hydrodynamic properties were not investigated. The phases were brought together at high speed through opposing nozzles. This configuration resulted in high turbulent mixing and overall mass transfer coefficients higher than in conventional contactors for similar power input. Saien and Moradi (2012) investigated the mass transfer performance of an impinging-jets mixer for a butanol succinic acid-water system at different nozzle diameters and distance, and jet velocities, and found improved mass transfer coefficients at reduced specific power input compared to other types of contactors. In a more recent work, Gao et al. (2016) investigated in confined impinging jets the effect of different operating conditions, such as flow rate ratio, nozzle diameter, and distance between the jet axes on the extraction of butyric acid using TBP and kerosene. Impinging-jets mixers have also been used for emulsifications (Siddiqui, 2014; Siddiqui and Norton, 2012). The effects of flow rates, type of emulsifier, and fluid properties on the mean drop size and the formation of small drops (<2 μm) were investigated with a laser diffraction system.

For the characterization of impinging-jets mixers of immiscible liquids it is important to know the sizes of the forming drops. Measurements can be particularly difficult at high dispersed phase fractions, while for unstable dispersions online measurement techniques are needed. One of the most common techniques to acquire drop size measurements in dispersed flows is imaging, particularly for low dispersed phase fractions (<0.1); at dense dispersions where there are multiple reflections and refractions it becomes difficult to distinguish the interfaces and measure the drop sizes. A number of other techniques have also been used including, among others, droplet encapsulation (Karabelas, 1978), electrozone sensing (Coulter Counter), local electrical probes (Lovick and Angeli, 2004), endoscope (Angeli and Hewitt, 2000), laser diffraction and laser back-scatter particle size analysers (Fang et al., 2009; Siddiqui and Norton, 2012; Simmons and Azzopardi, 2001), and focused beam reflectance probes (Wang et al., 2014).

The mixing intensity in the collision region of the impinging jets can be quantified by the specific energy dissipation rate, which is given by the kinetic energy change during the collision of the jets over the mixing volume in the impingement zone (Johnson and Prud'homme, 2003). Different approaches for the estimation of the energy dissipation rate have been reported in the literature. In the methodology suggested by Johnson (2003) and extended by Siddiqui et al. (2009) a macroscopic mechanical energy balance is carried out over the impingement zone, which includes the potential, kinetic, and pressure energy. The dissipation rate can also be found from the pressure drop measurements and the mechanical energy balance in the impinging-jets region (Zhou and Kresta, 1998a).

Impinging-jets mixers have the potential to generate liquid-liquid dispersions with small drop sizes and narrow distributions. However, the information available on the mixing of immiscible liquids in confined spaces is very limited. In this study, the effects of different geometries, jet velocities and phase flowrate ratios on the formation of dispersions of immiscible liquids and on drop size distribution are investigated. In addition, the average drop sizes are related to the energy dissipation rates in the impingement zone.

2. Experimental setup and conditions

The impinging-jets cell that was used to investigate the formation of liquid-liquid dispersions is shown in Fig. 1. The cell was made inside an acrylic block with flat surfaces using a CNC machine. Two side cylindrical channels, opposite to each other, were used as the cell inlets, from where the opposing jets entered the cell. Stainless steel nozzles with two different internal diameters (d_j), i.e. 0.25 and 0.5 mm, were inserted in the side channels. A
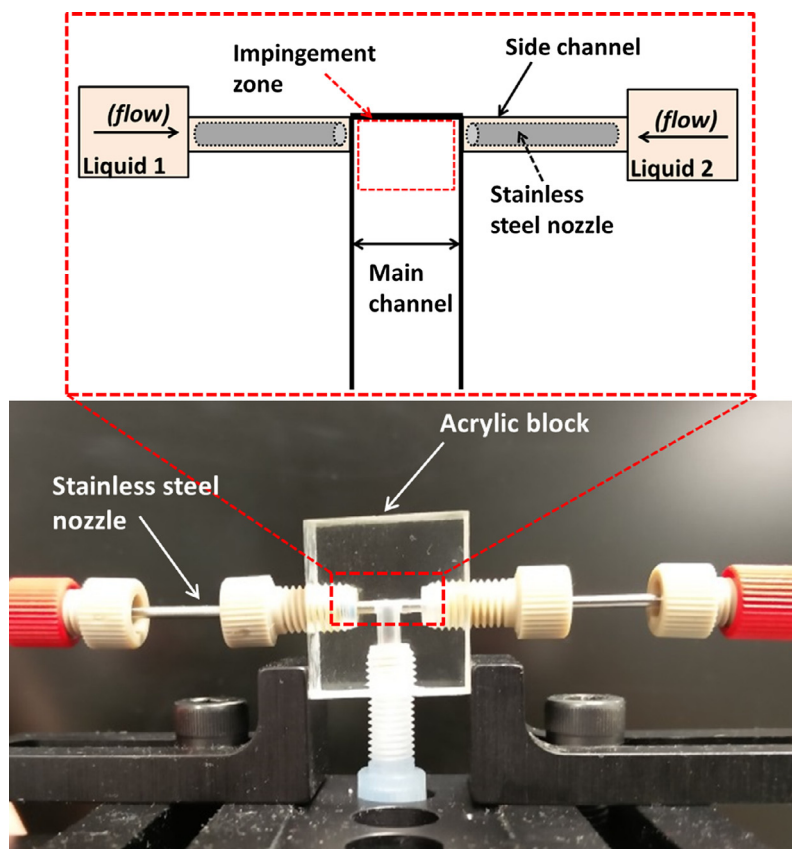
Fig. 1. Schematic diagram and photograph of the confined impinging-jets cell.

third circular channel in the acrylic block, perpendicular to the previous two but at the same plane, was used as the main channel (chamber) with internal diameter (D) of 2 or 3 mm. At the end of the main channel, an FEP tube was connected with internal diameter (D) the same as the main channel (i.e. 2 or 3 mm). The fluids were fed into the side channels using high-precision continuous syringe pumps (Harvard PHD Ultra), one for each liquid. Drop sizes were measured with a CMOS high-speed camera (Photron Fastcam-ultima APX), that has a maximum resolution of 1024×1024 at 2000 fps and is equipped with a magnification lens ($\times 12$, LEICA Monozoom 7 optical system). A micrometer stage, multi-axis platforms, and cross rollers were used for both the camera and the cell set up to allow a 3-D relative motion and precise alignment.

The measuring area was illuminated with a high power LED backlight. Drop sizes were measured in the impingement zone (Fig. 1), where the two jet streams collide, and also further downstream in the FEP tube. To minimise reflections and improve the images, a flat visualization box filled with water was used to enclose the FEP tube. The superficial velocity of each phase in the side jet channels ($u_j = Q/A$, where Q is the flowrate and A is the cross sectional area), varied between 0.17 and 6.2 m/s, while the volumetric flowrate ratio between the two phases, $r = Q_d/Q_c$ (Q_c and Q_d are the flow rates of the continuous and dispersed phase respectively), varied between 0.05 and 0.28. Both phases could become continuous depending on the phase flowrate ratio; for the range of flowrate ratios investigated, the fluid with the higher flow rate formed the continuous phase while the other was the dispersed. The Reynolds numbers ($Re_j = \rho_i u_j d_j / \mu_i$) of the jets varied from 40 to 2700, where ρ_i and μ_i is the density and viscosity of each liquid phase, respectively. The two test fluids used were deionised water, and Exxsol D80 (acquired from ExxonMobil) with

density of 795 kg/m^3 and dynamic viscosity at room temperature of 1.73 mPa s.

For the drop size distribution measurements it is important to acquire good images of the dispersion in the mixing zone and further downstream in the test channel. The quality of the images depended on the volume fraction of the dispersed phase and the mixture velocity, defined as $u_{mix} = \frac{Q_c + Q_d}{A}$, where A is the cross sectional area of the main channel. In Fig. 2, images acquired with the high-speed camera at low and intermediate phase ratios, $r = \frac{Q_d}{Q_c}$, where the organic is the dispersed phase, are shown. The acquired images were analysed using a post processing routine developed within an image analysis software (MIPAR). Each image was binarized using threshold pixel values to discriminate the dispersed
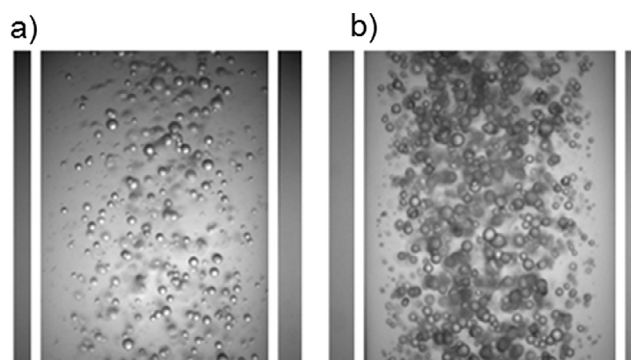

Fig. 2. Representative images taken with the high-speed camera for two different phase ratios before processing. Dispersed phase is organic. (a) r = 0.05, u_{mix} = 0.061 m/s; (b) r = 0.14, u_{mix} = 0.066 m/s.
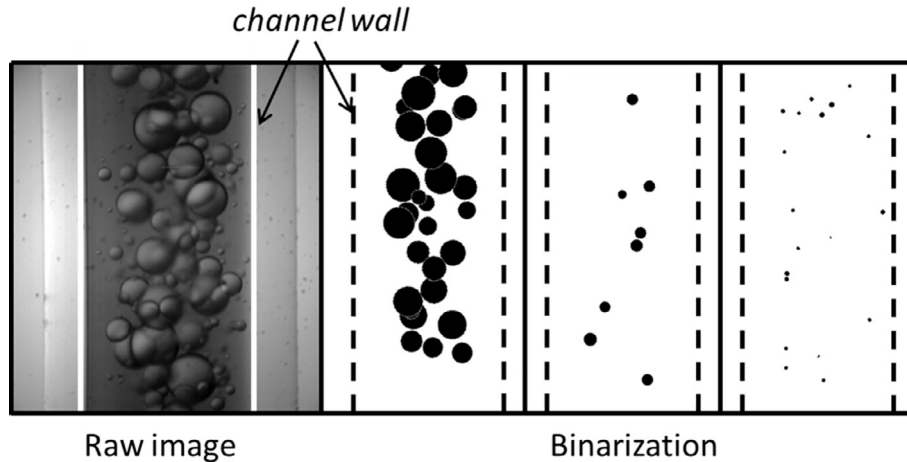
Fig. 3. Post-processing routine for measuring drop size distribution in the dispersions.

from the continuous phase (Fig. 3); subsequently drops were split into different size groups, whilst the number of groups depended on the drop size distribution.

From the drop size measurements the Sauter mean drop diameter, D[3,2], is calculated as follows:

$$D[3,2] = \frac{\sum_i^n d_i^3}{\sum_i^n d_i^2} \qquad (1)$$

where n is the number of drops, and d_i is the diameter of the drop i in the distribution.

The Sauter mean diameter (D[3,2]) represents the average size of the drops in a dispersion, but it does not reveal the spread or the shape of the distribution. In mass transfer operations it is desirable to have narrow drop size distributions because they ensure uniform conditions, while they help the design of separators for the two phases. It was found that the dispersions formed in the current impinging-jets system could be best fitted by two distributions, i.e. log normal and normal, depending on the continuous phase. Distributions were tested at 5% significance level.

When using image analysis to obtain drop size distributions it is important to measure the size of a sufficiently large number of drops. As shown in Fig. 4, the cumulative Sauter mean drop diameter D[3,2] becomes constant after about 450 counted drops for 3 indicative cases, covering a range of u_{mix} from 0.05 to 0.11 m/s. Meanwhile, the cumulative standard deviation decreases with increasing sample size. The standard deviation (σ), is calculated as

$$\sigma = \sqrt{\frac{\sum_{i=1}^n (d_i - D[1,0])^2}{n}} \qquad (2)$$

where D[1,0] is the arithmetic mean drop diameter, and was between 2 and 15% for all cases studied. Another important parameter is the polydispersity index (PdI) which is a measure of the width of the drop size distribution and of the uniformity of the drop size sample. The polydispersity index is defined as

$$PdI = \left(\frac{\sigma}{D[1,0]}\right)^2 \qquad (3)$$

3. Results and discussion

In this section, the effects of different operating conditions, main channel (chamber) size, jet diameter, and energy dissipation on drop size and drop size distribution are discussed, whilst the
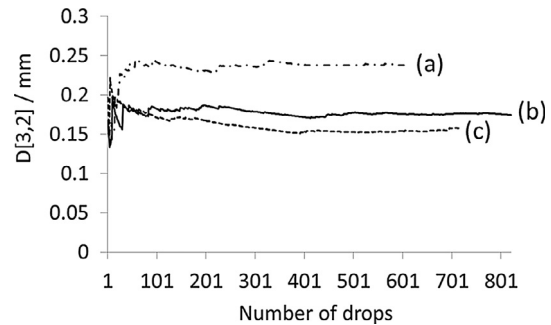

Fig. 4. Variation of Sauter mean drop diameter with the number of drops measured for r = 0.25. (a) u_{mix} = 0.05 m/s, (b) u_{mix} = 0.07 m/s, (c) u_{mix} = 0.11 m/s.

overall performance of the impinging-jets cell on the formation of dispersions is compared to that of other contactors.

3.1. Effect of total jet velocity and phase ratio on drop size

The effect of total jet velocity, $u_{j,t}$, defined as the sum of the jet velocities of the two phases, on the Sauter mean drop diameter is shown in Fig. 5 for two different dispersed to continuous phase flowrate ratios for the 2 mm main channel and for nozzle diameters (d_j) of 0.25 mm. The dispersed (organic) phase superficial jet velocities ($u_{j,d}$) varied between 0.3 and 1.4 m/s while those of the continuous (aqueous) phase, $u_{j,c}$, varied between 2 and 6 m/s. It can be seen that the mean drop size decreases with increasing total jet velocity for both phase ratios. In addition, for the whole range of total jet velocities, it was observed that the decrease followed a similar trend regardless of the phase ratio, while it resulted in similar drop sizes. This illustrates that the total jet velocity is the dominant parameter for drop formation. Similar decrease in drop size with total jet velocity was also observed when the large main channel was used (3 mm).

The effect of dispersed (organic) to continuous (aqueous) phase flowrate ratio on drop size at constant total jet velocity equal to 4 m/s is shown in Fig. 6 for individual jet velocities varying between 0.2 and 3.8 m/s. In general, the drop size increases with increasing dispersed phase ratio. The change is larger at low phase ratios where the size increases almost 3 times with an increase in phase ratio from 0.05 to 0.15. The increase is less (about 14%) at high phase ratios. By increasing the phase ratio, the energy dissipation rate in the collision zone of the two jets decreases and larger drops are formed, as will be shown in the following section. The
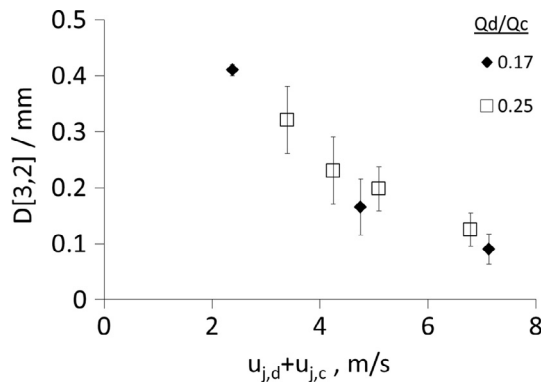
Fig. 5. Effect of total jet velocity on Sauter mean drop diameter at different dispersed (organic) to continuous (aqueous) phase ratios for D = 2 mm and d_j = 0.25 mm.
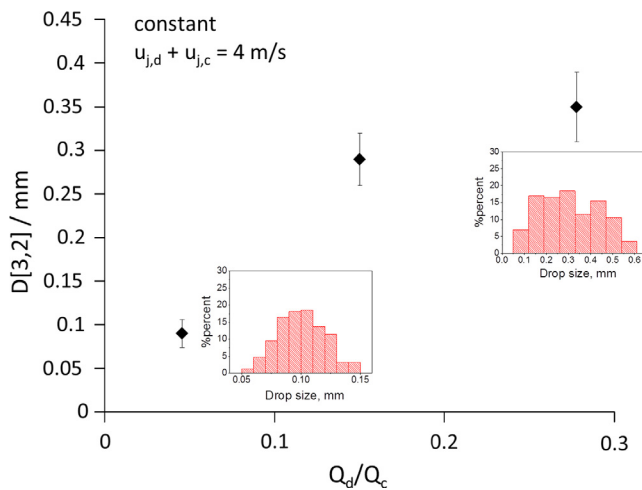

Fig. 6. Effect of dispersed (organic) to continuous (aqueous) phase ratios on Sauter mean drop diameter at constant total jet velocity 4 m/s (D = 2 mm, d_j = 0.25 mm).

drop size distributions were also found to be affected by the phase ratio; at phase ratio 0.05, a very narrow drop size distribution is obtained ranging from 0.05 to 0.14 mm, whilst at phase ratio 0.28, the distribution is wider and extends from 0.05 to 0.6 mm (insets in Fig. 6). However, the percentage of small drops (in the range of 0.05 and 0.1 mm) in the case of the high phase ratio is low. Similar results were also found in the large 3 mm main channel.

The interfacial area (α) is an important parameter for dispersed flow applications in mass transfer. The interfacial area can be calculated from the Sauter mean diameter D[3,2] as follows (Shi et al., 2015):

$$\alpha = \frac{6\varphi}{D[3,2]} \tag{4}$$

where φ is the volume fraction of the dispersed phase ($\varphi = \frac{Q_d}{Q_d + Q_c}$). The variation of interfacial area with total jet velocity is shown in Fig. 7 for the 2 and 3 mm main channels and all phase ratios tested (0.05–0.28). As can be seen, the interfacial areas depend mainly on the jet total velocity whilst, the effect of phase ratio is relatively small. For example, in the case of the 2 mm channel at total jet velocity 4 m/s, the interfacial area decreased only by 23% for a phase ratio decrease from 0.28 to 0.05 (82% decrease). The interfacial area followed similar trends with the total jet velocity for both channel sizes, and varied between 2000 and 11,500 m²/m³. The
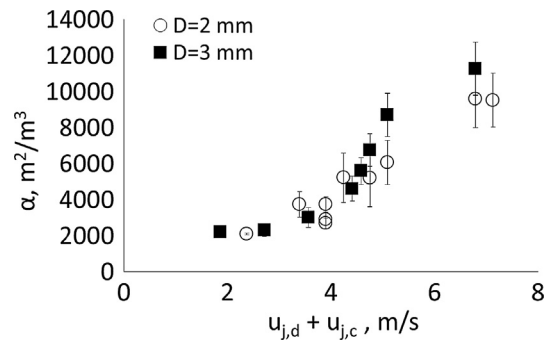
increase in interfacial area at total jet velocities from 2 to 4 m/s is small for both cells, whilst beyond 4 m/s it increases significantly. Interfacial areas are comparable for both cells at total jet velocities up to about 5 m/s, while beyond this velocity higher values of interfacial areas are obtained in the large cell. The Re_j of the continuous phase for these cases in the 3 mm channel reached up to 2700 and is higher than in the 2 mm channel. High continuous phase Re leads to the formation of small drops and hence large interfacial area. The values of interfacial area obtained are one to two orders of magnitude higher than the interfacial areas obtained in conventional liquid-liquid contactors, such as stirred vessels (Fernandes and Sharma, 1967) or packed bed columns (Verma and Sharma, 1975), and almost three times higher than in intensified capillary contactors (0.5–2 mm ID, (Tsaoulidis and Angeli, 2016); 0.5–1 mm ID, (Kashid et al., 2007)). They are also higher compared to interfacial areas previously reported in the literature for two impinging-jets reactors, which varied from 350 to 900 m²/m³ and calculated using the chemical method (d_j = 1 mm, 1.5 mm internozzle distance, (Dehkordi, 2002)).

The effect of phase ratio on drop size and interfacial area is presented in Fig. 8 for the 3 mm channel and 0.5 mm jet diameters for either the dispersed or the continuous phase jet velocity constant. In all these conditions, the organic phase forms the dispersed drops. As expected, there is an increase in drop size as the dispersed to continuous phase ratio increases in both cases. However, the increase follows different trends; when the dispersed phase jet velocity is constant the increase in drop size is large; for example, the drop size increases by 2.5 times when the phase ratio increases from 0.05 to 0.1. When the continuous phase jet velocity is constant, on the other hand, the increase in drop size with phase ratio
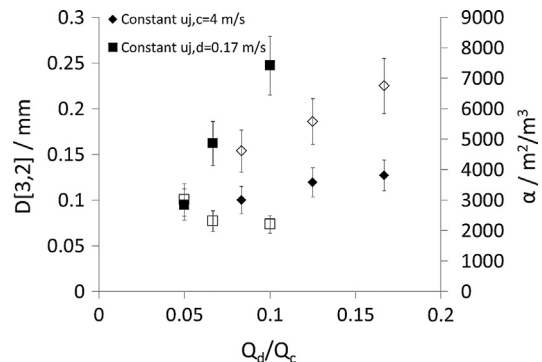

Fig. 7. Effect of total jet velocity on interfacial area (α) at dispersed (organic) to continuous (aqueous) phase ratios (r = Q_d/Q_c) from 0.05 to 0.28 in the 2 and 3 mm channels.

Fig. 8. Effect of dispersed (organic) to continuous (aqueous) phase ratio on Sauter mean drop diameter for constant dispersed or continuous phase jet velocity (D = 3 mm, d_j = 0.5 mm). Filled symbols correspond to the D[3,2] axis, whilst empty symbols correspond to the interfacial area (α) axis.
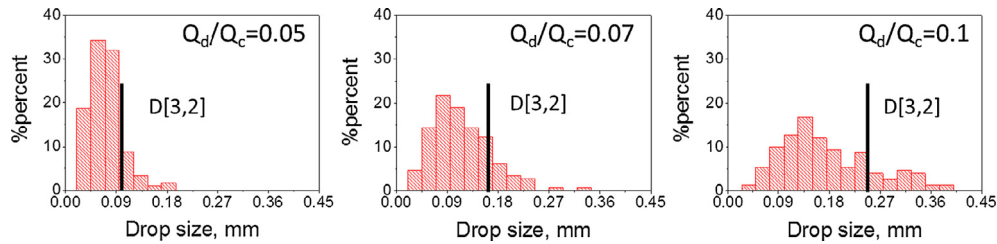
Fig. 9. Effect of dispersed (organic) to continuous (aqueous) phase ratio on drop size distribution for dispersed phase jet velocity $u_{j,d}$ = 0.17 m/s (D = 3 mm, d_j = 0.5 mm).
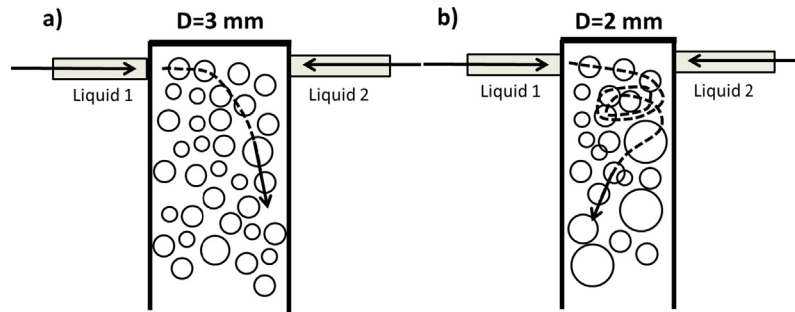

Fig. 10. Schematic representation of the path the drops follow within the two channels at low jet velocities.

is small. This is attributed, as discussed before, to the dominant effect of total jet velocity on drop size. When $u_{j,c}$ is constant, an increase in the ratio is associated with a small change in the total jet velocity from 4.4 to 4.8 m/s, while when $u_{j,d}$ is constant an increasing ratio is associated with significant decrease of the total jet velocity from 3.6 to 1.9 m/s.

The interfacial area (α) also follows a different trend in the two cases. At constant $u_{j,d}$ there is a slight decrease in (α) with increasing phase ratio, whilst at constant $u_{j,c}$ there is a large increase. It was also found that drops were more uniform (average PdI = 0.12) when the continuous phase jet velocity was kept constant, than when the dispersed phase jet velocity was constant (average PdI = 0.18).

The effect of phase ratio on the drop size distribution is shown in Fig. 9 for different continuous (aqueous) phase jet velocities and constant dispersed phase jet velocity (black squares in Fig. 8). By increasing the dispersed to continuous phase flowrate ratio, the drop size increases and the distribution becomes wider. It can also be seen that by increasing the phase ratio the percentage of small drops decreases, while the percentage of large drops increases. The high percentage of small drops at phase ratio 0.05 is associated with the high Re number of the continuous phase (high Q_c) which affects the deformation and breakup of the dispersed phase.

3.2. Effect of main channel (chamber) size

To investigate the effect of the main channel size on drop formation, two different channel diameters were used (2 and 3 mm), whilst the nozzle diameter was the same (d_j=0.25 mm). The continuous phase jet velocity varied from 2.8 to 5.44 m/s, and the dispersed phase jet velocity was between 0.68 and 1.36 m/s. It was found that the chamber size influenced the drop size because it affected the flow field in the impingement zone (Fig. 10) and the shape of the formed liquid jets (Fig. 11), especially at low jet velocities. In the small channel (D = 2 mm) at low jet velocities, drops detached from the end of the jet (Fig. 11a) at diameters larger than the jet diameter. In addition, the drops, instead of flowing away, circulated in the impingement cell (Fig. 10b), which increased their rate of collision with other drops
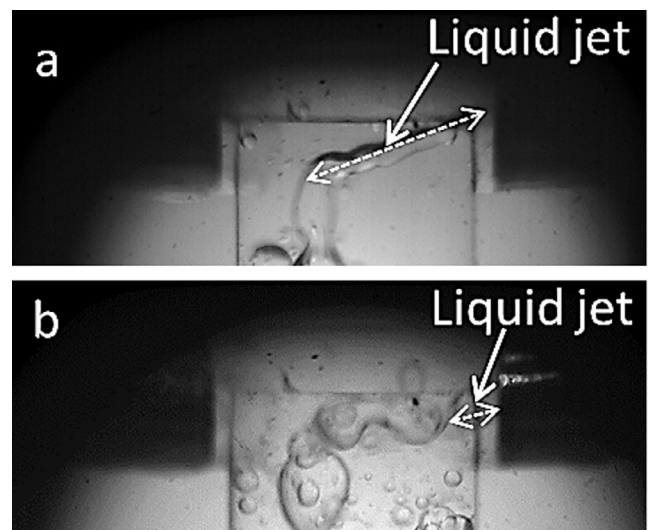

Fig. 11. Typical photographs of the shape of the liquid jet at (a) low and (b) high jet velocities.

and resulted in coalesce that gave larger drops and a wider drop size distribution. This was not observed however, in the large channel where the drops flowed directly away from the impingement zone (Fig. 10a). At high jet velocities in both channels, the dispersed phase jet destabilised immediately after exiting the nozzle tip (Fig. 11b) and once formed, the drops flowed downwards from the impingement zone.

The effect of main channel size on the drop size distribution is shown in Fig. 12, for the lowest and highest dispersed phase jet velocity, 0.68 m/s and 1.36 m/s, respectively. At low jet velocities (Fig. 12a and c) the drop size distribution is wider in the small channel (drop sizes between 0.05 and 0.55 mm), than in the large one (drop sizes between 0.03 and 0.40 mm), and the Sauter mean diameter is larger. At high jet velocities (Fig. 12b and d), the drop size distributions are narrow for both channels. The drops are
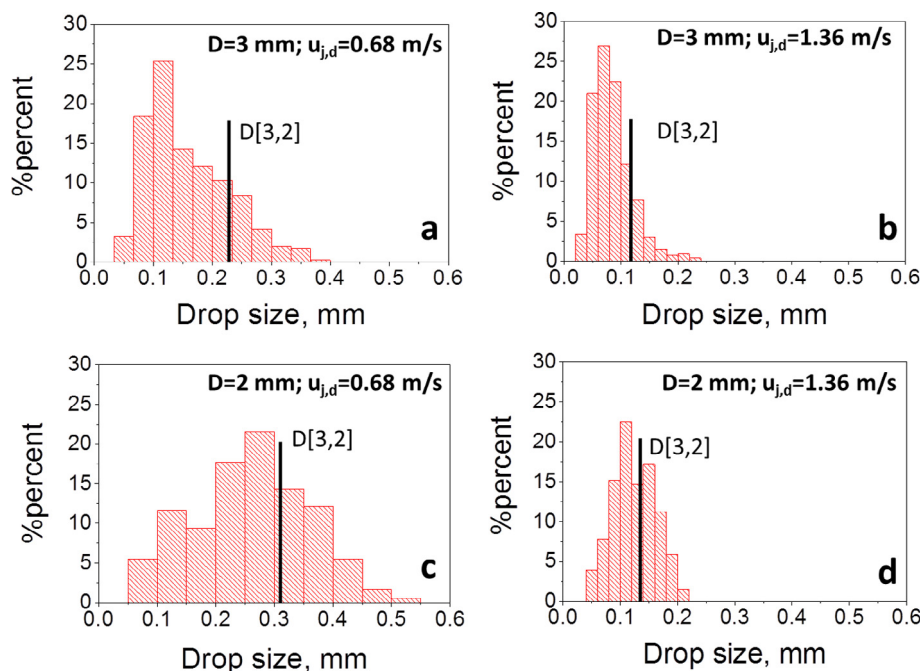
Fig. 12. Effect of main channel size and jet velocity of the dispersed (organic) phase on drop size distribution (d_j = 0.25 mm, r = Q_d/Q_c = 0.25).

smaller than the diameter of the jet in both cases, with sizes varying between 0.04 and 0.23 mm. Although the drop size distribution was wider for some cases in the 2 mm channel compared to the 3 mm one, in general the PdIs were similar; the PdI varied between 0.12 and 0.19 in the 2 mm channel, and between 0.10 and 0.18 in the 3 mm channel.

The Sauter mean diameters in both channels are shown in Fig. 13 for a flowrate ratio equal to 0.25. The difference between the drop sizes is large at low dispersed phase jet velocities, and decreases significantly at high jet velocities. The interfacial area increased with increasing dispersed phase jet velocity for both channel sizes, whilst on average the interfacial areas were ~20% higher in the large channel compared to the small one.

3.3. Effect of nozzle diameter

The effect of nozzle diameter (d_j) on drop size was also investigated for two nozzle sizes equal to 0.25 and 0.5 mm, under the same jet velocities. The jet velocities varied from 0.85 to 5.44 m/s. The drop size distributions for the 3 mm channel are shown in Fig. 14 for increasing dispersed phase jet velocity at phase ratio
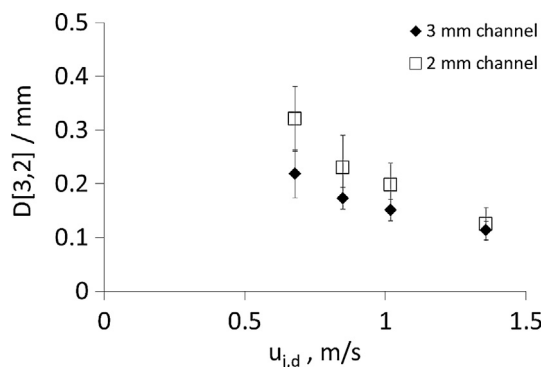

Fig. 13. Effect of main channel size on Sauter mean drop diameter at different dispersed phase jet velocities (d_j = 0.25 mm, r = Q_d/Q_c = 0.25).

equal to 0.25. As can be seen, the D[3, 2] did not vary significantly, but the polydispersity index (PdI) was lower with the 0.5 mm nozzle compared to the 0.25 mm one for the same conditions. This can be explained by the formation of satellite droplets with the small nozzles because the jet expands as it emerges from the nozzle for this case. As can be seen in Fig. 14, the percentage of fine drops (<0.08 mm) in the case of the 0.25 mm nozzle size at all conditions examined is larger than that of the 0.5 mm. For both nozzles, the distributions are shifted to smaller drops at the left and the polydispersity index (PdI) decreases as the jet velocity increases. Drops formed with the large nozzle have sizes almost 3 times smaller than the diameter of the nozzle. At the high jet velocity ($u_{j,d}$ = 1.36 m/s), drops formed with the small nozzle have sizes smaller than the nozzle diameter as well.

3.4. Effect of continuous phase

Drop sizes were also measured when the aqueous phase was dispersed. As can be seen in Fig. 15, when the aqueous phase is dispersed, the average drop size is almost 4 times larger than when the organic phase is dispersed under the same conditions (jet velocity, flowrate phase ratio). The formation of drops is a result of the deformation of the jet of the dispersed phase during the collision of the two phases in the impingement zone. Thus, the higher the Reynolds number of the continuous phase the higher the external inertial stresses that tend to deform the jet and create small drops. When the aqueous is the continuous phase, the continuous phase Re varies between 678 and 1360, whilst when the organic is the continuous phase, Re varies between 319 and 637. The results also indicate that when the aqueous phase is dispersed, the dispersed phase jet velocity ($u_{j,d}$) affects the drop size more than when the organic phase is dispersed. In addition, when the aqueous phase is dispersed the polydispersity index is lower (PdI = 0.05) than when the organic phase is dispersed. The effect of total jet velocity on drop size distribution for aqueous dispersed phase is shown in Fig. 16 at phase flowrate ratio equal to 0.25. As expected, the distribution is shifted to the right as the jet velocity decreases and bigger drops form.
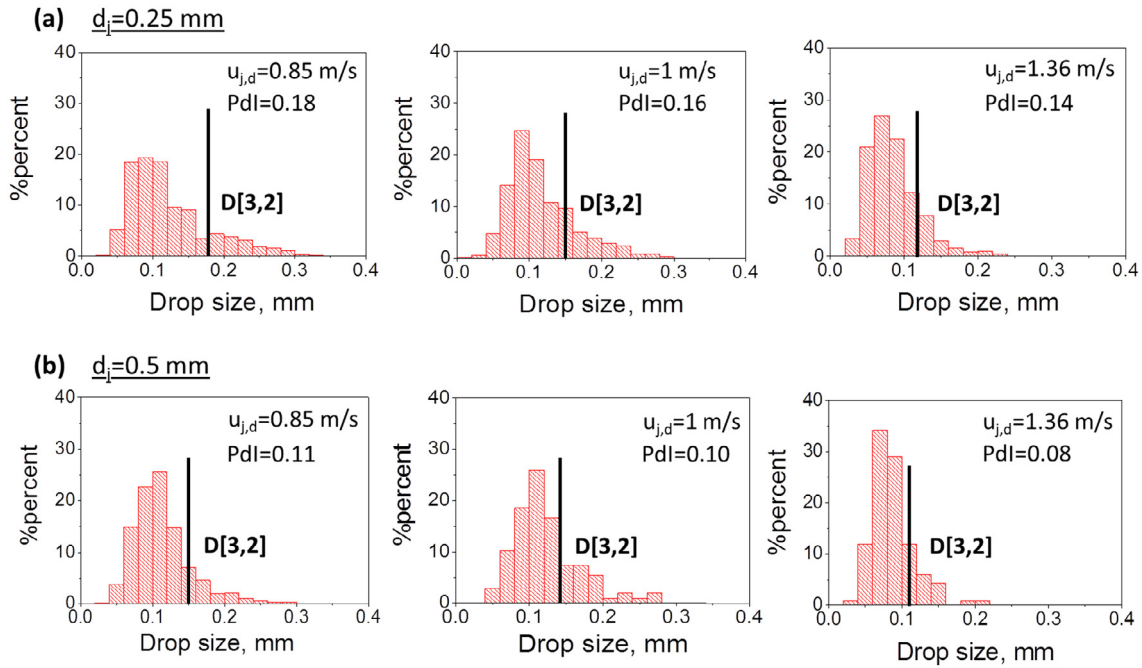
(a) $\underline{d_j=0.25 \text{ mm}}$

(b) $\underline{d_j=0.5 \text{ mm}}$

Fig. 14. Effect of nozzle diameter (d_j) on Sauter mean drop diameter and on drop size distribution at different dispersed phase jet velocities at r = 0.25 and D = 3 mm.

3.5. Drop size evolution along the channel

The dispersions formed are not stable and the drop size can change in the main channel downstream the jet impingement zone due to breakage and coalescence phenomena. To study the evolution of drop size, measurements were taken for water continuous dispersions in three axial locations; in the jet impingement zone and at two further positions downstream, L/D = 7.5 and L/D = 15, respectively, where L is the channel length. The Sauter mean drop size at the different locations is shown in Fig. 17 for the 2 mm main channel and both jet diameters equal to d_j = 0.25 mm. The results are plotted as a function of mixture velocity in the main channel, which is expected to affect the evolution of the drop size. The phase ratio was kept constant at 0.17. As can be seen, at the low mixture velocity the average drop size increases downstream, which suggests that coalescence takes place after the impingement zone. The increase in drop size happens within the first part of the test section (up to L/D = 7.5) while after that the average drop size does not change. At the high velocities, the average drop size does not change along the channel length investigated.

The drop size distributions in the mixing zone and at L/D = 7.5 for the low mixture velocity (0.037 m/s) are shown in Fig. 18. Although the width of the distribution is similar in both cases, with drop sizes ranging from ~0.1 to ~0.6 mm, in the mixing zone higher percentage of drops have smaller sizes than in L/D = 7.5. About 90% of the drop sizes obtained in the mixing zone are below 0.45 mm, whilst at L/D = 7.5 only 70% of the drop sizes are below 0.45 mm.

Average profiles of the drop velocity (u_d) normalised against the mixture velocity for 3 different mixture velocities and phase ratio equal to 0.17 are shown in Fig. 19. Velocity data were obtained at L/D = 7.5 since no change on the average drop size was noticed further downstream. The results indicate that drops flow at different velocities depending on their radial position, whilst there is symmetry to the channel centreline. Close to the channel centre drops move faster than the mixture velocity, while close to the wall they are moving with lower velocity than the mixture. The drop velocity

will affect their residence time in the channel, which is important for mass transfer applications.

The relationship between D[3,2] and the maximum drop diameter (D_{max}) is presented in Fig. 20 for all cases investigated. D_{max} was taken equal to D_{95}, the diameter corresponding to 95% of the cumulative drop volume curve. A proportionality coefficient between the two diameters close to unity implies a very narrow distribution. It was found that this coefficient is not constant for the whole range of conditions investigated, although it does not vary significantly, i.e. 0.68–0.82. The proportionality coefficient is higher when the aqueous is the dispersed phase. In both cases, however, the proportionality coefficients are higher to those found in stirred tanks (Zhou and Kresta, 1998a) and static mixers ((Berkman and Calabrese, 1988), where the coefficients vary between 0.42 and 0.69. The values of the coefficients were independent of the main channel size and the nozzle diameters.

In most cases, the Sauter mean diameter is related to the shape of the drop size distribution. Researchers have used various distributions to fit their experimental data (Angeli and Hewitt, 2000; Calabrese et al., 1986; Simmons, 1977; Sprow, 1967; Tavlarides and Stamatoudis, 1981), with the log-normal and normal distributions the ones used commonly. In the current study the cumulative drop size distributions were found to be best described by a log-normal function when the organic phase is dispersed in the 3 mm channel, whilst in the other two cases, i.e. organic phase dispersed in the 2 mm channel and aqueous phase dispersed in the 3 mm channel, the distributions were best described by the normal function.

The change on drop size as a function of the specific energy dissipation rate (ε) in the impingement zone for the two different main channel sizes (2 mm and 3 mm), the two nozzle diameters (0.25 mm and 0.5 mm), and phase ratios varying from 0.05 to 0.28 is shown in Fig. 21. The value of (ε) in the impingement zone is estimated following the works by Siddiqui et al. (2009) and Mahajan and Kirwan (1996), as follows:

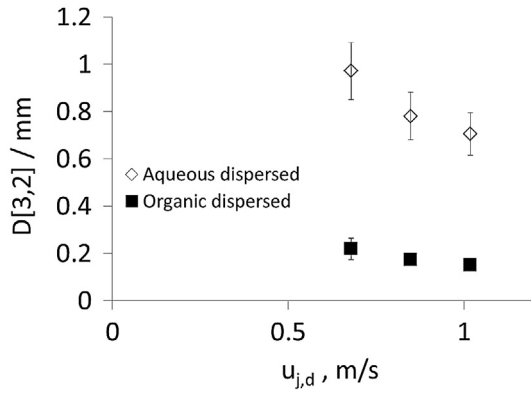$$\varepsilon = \frac{P_k}{\rho V_{iz}} \qquad (5)$$

Fig. 15. Effect of dispersed phase jet velocity on the Sauter mean drop diameter for different continuous phases in the 2 mm channel at dispersed to continuous phase ratio of 0.25.

where V_{iz} is the volume of the impingement zone and ρ is the density of the mixture. The rate of the kinetic energy input (P_k) can be expressed as

$$P_k \propto \frac{\dot{m}_d u_{j,d}^2}{2} + \frac{\dot{m}_c u_{j,c}^2}{2} \tag{6}$$

where $\dot{m}_d$ and $\dot{m}_c$ are the mass flowrates (kg/s), whilst $u_{j,d}$ and $u_{j,c}$ are the superficial velocities (m/s) of the opposing jets of the dispersed and the continuous phase respectively. The two immiscible jets collide in the cell and the velocities are redirected. The kinetic energy associated with each stream is dissipated within a very small volume and induces a turbulent-like motion which intensifies the mixing and in the case of immiscible liquids enhances the breakage of drops. Normally, the zone where mixing is intense (impingement zone) is limited to a small region of the total volume of the impinging-jets cell. In addition, the volume of this zone for a particular cell configuration fluctuates depending on the Re_j. Here, the volume V_{iz} is taken as the volume of a cylinder with height equal to its diameter, and equal to the diameter of the channel. As can be seen from Fig. 21, in general, the Sauter mean drop diameter decreases with increasing specific energy dissipation rate. When the organic phase is dispersed the same energy dissipation rate resulted in smaller average drop sizes in the 3 mm channel compared to the 2 mm one, particularly at the low energy dissipation rates, where the continuous phase Re in the 3 mm channel is higher than in the 2 mm one. At high energy dissipations rates the average drop sizes reach the same minimum value regardless of the channel size. In addition, the drop size decreases faster in the small channel compared to the large one. At low values of (ε) it is observed that for the same energy dissipation rates, larger

Fig. 17. Effect of main channel length on Sauter mean drop diameter at different mixture velocities in the 2 mm channel. (d_j = 0.25 mm, $u_{j,t}$ = 2.4–7.1 m/s, r = 0.17).

drops form when the organic is the continuous phase in the 3 mm channel, which is attributed to the lower Re_c than when the aqueous is the continuous phase. As can also be seen in Fig. 21 (inset) the nozzle diameter does not affect the average drop size for the same energy dissipation rates. The Sauter mean average drop diameter can be related to the specific energy dissipation rate as follows

$$D[3,2] = k\varepsilon^{-b} \tag{7}$$

The value of the power [b] varies between 0.21 and 0.43 (Fig. 21). The dependency of the Sauter mean drop diameter and drop size distribution on the specific energy dissipation rate has also been investigated previously for different liquid-liquid contactors (Zhou and Kresta, 1998b). From investigations of the emulsification processes of sunflower/water system with added surfactants in an impinging-jets device Siddiqui and Norton (2012) reported that the power [b] varied between 0.094 and 0.358. In stirred tanks for different viscosity systems, Aldana (2005) found that the power of [b] was between 0.07 and 0.48, whilst Davies (1987) found a value of 0.4.

4. Conclusions

The formation of liquid-liquid dispersions in an impinging-jets mixer was studied experimentally. The jets were formed in two opposing channels with the same internal diameter of either 0.25 or 0.5 mm, and collided in a main channel with internal diameter of either 2 or 3 mm, which was perpendicular to the previous two. Both aqueous and organic continuous dispersions were formed depending of the flowrate ratio of the two phases. Drop sizes were studied in the mixing zone and further downstream with high speed imaging.

It was found that the drop size was mainly affected by the total velocity of the two jets, while the effect of the flowrate ratio of the two phases was not as significant. In addition, the interfacial area
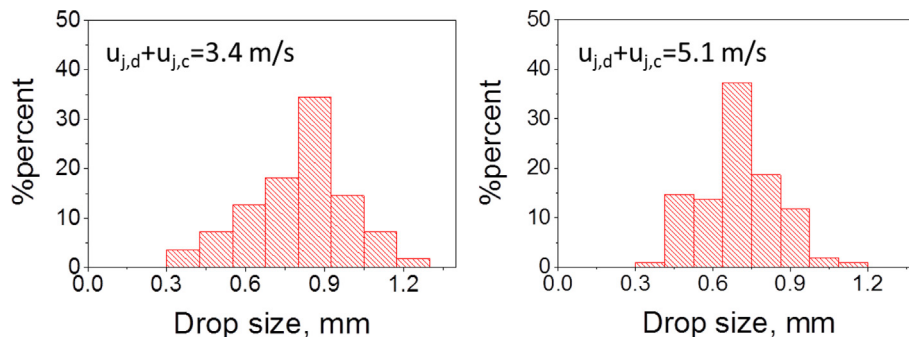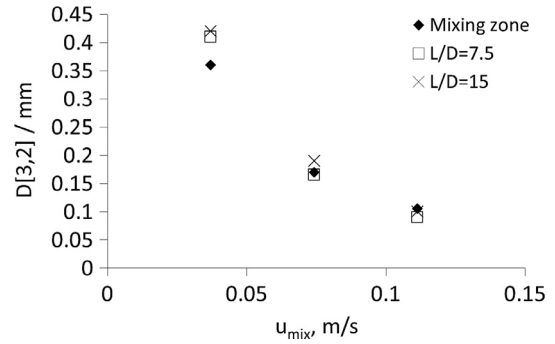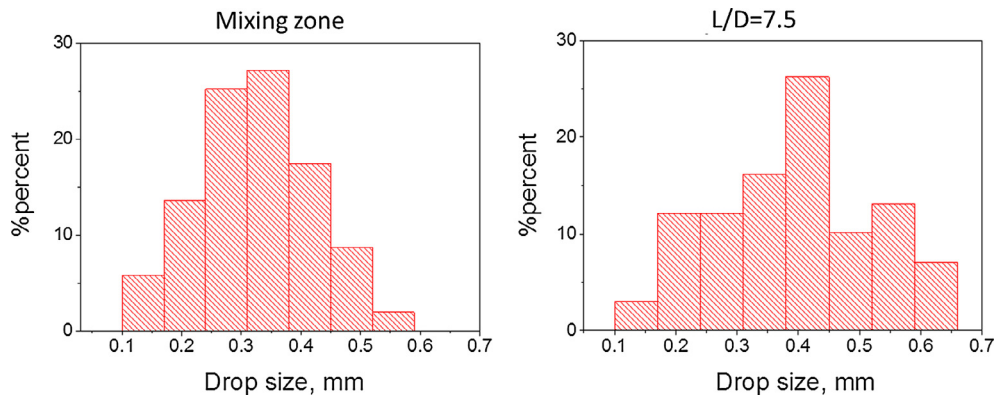

Fig. 16. Effect of total jet velocity on drop size distribution when the organic is the continuous phase, at dispersed to continuous phase ratio r = 0.25. (D = 2 mm, d_j = 0.25 mm).

Fig. 18. Drop size distribution in the impingement zone of the jets and at a downstream location of L/D = 7.5, for mixture velocity 0.037 m/s and r = 0.17. (D = 2 mm, d_j = 0.25 mm).
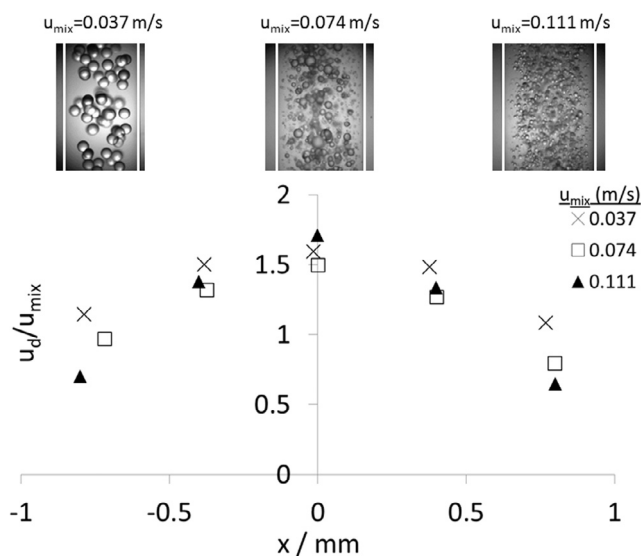

Fig. 19. Profiles of the drop velocity u_d normalized with the mixture velocity at L/D = 7.5 in the 2 mm channel at phase ratio 0.17 ($u_{j,c}$ = 2–6 m/s and $u_{j,d}$ = 0.34–1 m/s, d_j = 0.25 mm).

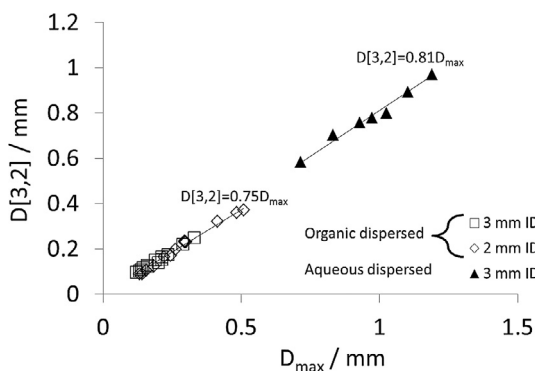**Fig. 20.** Sauter mean drop diameter as a function of D_{max} for all the cases studied.

Fig. 21. Effect of specific energy dissipation rate (ε) on Sauter mean drop diameter for all cases studied.

increased with increasing total jet velocity. The impinging-jets mixer produced interfacial areas almost three times larger than capillary contactors at similar mixture velocities, and up to two orders of magnitude larger than conventional contactors.

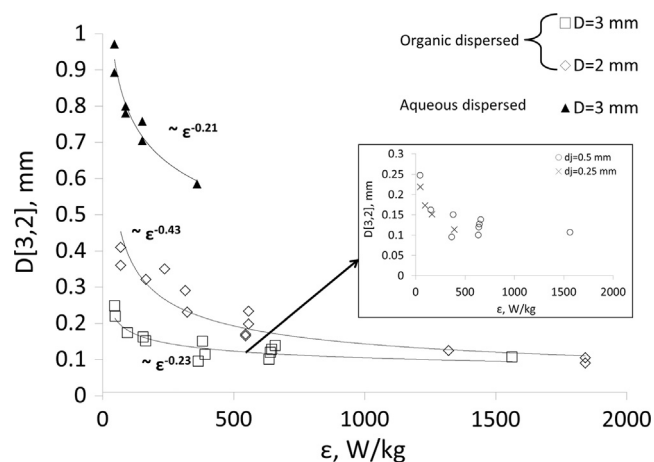Drop sizes were in general larger in the organic than in the aqueous continuous dispersions. In addition, the PdI in the impinging-jets cell had an average value of 0.13 in the aqueous continuous dispersions, and 0.05 in the organic continuous dispersions, indicating a very narrow distribution. The size of the main channel also affected the drop size and, interestingly, smaller drops were formed in the large channel compared to the small one, which is important for scale up purposes. For the conditions investigated, the drop sizes did not change significantly at distances equal to 15 channel diameters downstream the impingement area. The drops acquired a parabolic profile as they were flowing in the main channel, which affects their residence time. The Sauter mean drop diameter was found to decrease with increasing specific energy dissipation rate in the impingement zone, following a relation of the form $\sim\varepsilon^{-b}$. At low energy dissipation rates the drop size depended on the phase flowrate ratio and main channel size, whilst there was no obvious effect at higher ε values.

The current results indicate that impinging-jets cells can generate small drop sizes with narrow distributions at high throughputs. Further studies will explore the effects of different fluids properties and of a wider range of geometrical characteristics on the performance of the impinging-jets mixer.

References

Aldana, G.A.P., 2005. Effect of Surfactants on Drop Size Distributions in a Batch, Rotor-Stator Mixer. UMI.

Angeli, P., Hewitt, G.F., 2000. Drop size distributions in horizontal oil-water dispersed flows. Chem. Eng. Sci. 55, 3133–3143.

Berkman, P.D., Calabrese, R.V., 1988. Dispersion of viscous liquids by turbulent flow in a static mixer. AIChE J. 34, 602–609.

Calabrese, R., Wang, C., Bryner, N., 1986. Drop breakup in turbulent stirred-tank contactors. Part III: Correlations for mean size and drop size distribution. AIChE J. 32, 677–681.

Chen, H.T., Middleman, S., 1967. Drop size distribution in agitated liquid-liquid systems. AIChE J. 13, 989–995.

Das, M.D., Hrymak, A.N., Baird, M.H., 2013. Laminar liquid–liquid dispersion in the SMX static mixer. Chem. Eng. Sci. 101, 329–344.

Daub, A., Böhm, M., Delueg, S., Büchs, J., 2013. Measurement of maximum stable drop size in aerated dilute liquid–liquid dispersions in stirred tanks. Chem. Eng. Sci. 104, 147–155.

Davies, J., 1987. A physical interpretation of drop sizes in homogenizers and agitated tanks, including the dispersion of viscous oils. Chem. Eng. Sci. 42, 1671–1676.

Dehkordi, A.M., 2001. Novel type of impinging streams contactor for liquid-liquid extraction. Ind. Eng. Chem. Res. 40, 681–688.

Dehkordi, A.M., 2002. Liquid-liquid extraction with an interphase chemical reaction in an air-driven two-impinging-streams reactor: effective interfacial area and overall mass-transfer coefficient. Ind. Eng. Chem. Res. 41, 4085–4093.

Fang, J.-Y., Hung, C.-F., Hua, S.-C., Hwang, T.-L., 2009. Acoustically active perfluorocarbon nanoemulsions as drug delivery carriers for camptothecin: drug release and cytotoxicity against cancer cells. Ultrasonics 49, 39–46.

Fernandes, J., Sharma, M., 1967. Effective interfacial area in agitated liquid—liquid contactors. Chem. Eng. Sci. 22, 1267–1282.

Fonte, C.P., Sultan, M.A., Santos, R.J., Dias, M.M., Lopes, J.C.B., 2015. Flow imbalance and Reynolds number impact on mixing in Confined Impinging Jets. Chem. Eng. J. 260, 316–330.

Gao, Z., Han, J., Xu, Y., Bao, Y., Li, Z., 2013. Particle Image Velocimetry (PIV) investigation of flow characteristics in confined impinging jet reactors. Ind. Eng. Chem. Res. 52, 11779–11786.

Gao, Z., Zhao, M., Yu, Y., Li, Z., Han, J., 2016. Investigation of extraction fraction in confined impinging jet reactors for tri-butyl-phosphate extracting butyric acid process. Chin. J. Chem. Eng. 24, 310–316.

Icardi, M., Gavi, E., Marchisio, D.L., Barresi, A.A., Olsen, M.G., Fox, R.O., Lakehal, D., 2011. Investigation of the flow field in a three-dimensional Confined Impinging Jets Reactor by means of microPIV and DNS. Chem. Eng. J. 166, 294–305.

Johnson, B.K., 2003. Flash nanoprecipitation of organic actives via confined micromixing and block copolymer stabilization.

Johnson, B.K., Prud'homme, R.K., 2003. Chemical processing and micromixing in confined impinging jets. AIChE J. 49, 2264–2282.

Karabelas, A., 1978. Droplet size spectra generated in turbulent pipe flow of dilute liquid/liquid dispersions. AIChE J. 24, 170–180.

Kashid, M.N., Harshe, Y.M., Agar, D.W., 2007. Liquid-liquid slug flow in a capillary: an alternative to suspended drop or film contactors. Ind. Eng. Chem. Res. 46, 8420–8430.

Lee, L., Norton, I.T., 2013. Comparing droplet breakup for a high-pressure valve homogeniser and a microfluidizer for the potential production of food-grade nanoemulsions. J. Food Eng. 114, 158–163.

Lemenand, T., Della Valle, D., Zellouf, Y., Peerhossaini, H., 2003. Droplets formation in turbulent mixing of two immiscible fluids in a new type of static mixer. Int. J. Multiph. Flow 29, 813–840.

Lovick, J., Angeli, P., 2004. Droplet size and velocity profiles in liquid–liquid horizontal flows. Chem. Eng. Sci. 59, 3105–3115.

Maaß, S., Wollny, S., Voigt, A., Kraume, M., 2011. Experimental comparison of measurement techniques for drop size distributions in liquid/liquid dispersions. Exp. Fluids 50, 259–269.

Mahajan, A.J., Kirwan, D.J., 1996. Micromixing effects in a two-impinging-jets precipitator. AIChE J. 42, 1801–1814.

Metzger, L., Kind, M., 2016. On the mixing in confined impinging jet mixers – Time scale analysis and scale-up using CFD coarse-graining methods. Chem. Eng. Res. Des. 109, 464–476.

Parhizkar, M., Edirisinghe, M., Stride, E., 2013. Effect of operating conditions and liquid physical properties on the size of monodisperse microbubbles produced in a capillary embedded T-junction device. Microfluid. Nanofluid. 14, 797–808.

Saien, J., Moradi, V., 2012. Low interfacial tension liquid–liquid extraction with impinging-jets contacting method: influencing parameters and relationship. J. Ind. Eng. Chem. 18, 1293–1300.

Saien, J., Zonouzian, S.A.E., Dehkordi, A.M., 2006. Investigation of a two impinging-jets contacting device for liquid–liquid extraction processes. Chem. Eng. Sci. 61, 3942–3950.

Shi, D., Sadat, M.E., Dunn, A.W., Mast, D.B., 2015. Photo-fluorescent and magnetic properties of iron oxide nanoparticles for biomedical applications. Nanoscale 7, 8209–8232.

Siddiqui, S.W., 2014. The effect of oils, low molecular weight emulsifiers and hydrodynamics on oil-in-water emulsification in confined impinging jet mixer. Colloids Surf., A 443, 8–18.

Siddiqui, S.W., Norton, I.T., 2012. Oil-in-water emulsification using confined impinging jets. J. Colloid Interface Sci. 377, 213–221.

Siddiqui, S.W., Zhao, Y., Kukukova, A., Kresta, S.M., 2009. Characteristics of a confined impinging jet reactor: energy dissipation, homogeneous and heterogeneous reaction products, and effect of unequal flow. Ind. Eng. Chem. Res. 48, 7945–7958.

Simmons, H., 1977. The correlation of drop-size distributions in fuel nozzle sprays—Part I: The drop-size/volume-fraction distribution. J. Eng. Power 99, 309–314.

Simmons, M., Azzopardi, B., 2001. Drop size distributions in dispersed liquid–liquid pipe flow. Int. J. Multiph. Flow 27, 843–859.

Sprow, F., 1967. Distribution of drop sizes produced in turbulent liquid—liquid dispersion. Chem. Eng. Sci. 22, 435–442.

Sultan, M.A., Fonte, C.P., Dias, M.M., Lopes, J.C.B., Santos, R.J., 2012. Experimental study of flow regime and mixing in T-jets mixers. Chem. Eng. Sci. 73, 388–399.

Tavlarides, L.L., Stamatoudis, M., 1981. The analysis of interphase reactions and mass transfer in liquid-liquid dispersions. Adv. Chem. Eng. 11, 199–273.

Tsaoulidis, D., Angeli, P., 2016. Effect of channel size on liquid-liquid plug flow in small channels. AIChE J. 62, 315–324.

Verma, R., Sharma, M., 1975. Mass transfer in packed liquid—liquid extraction columns. Chem. Eng. Sci. 30, 279–292.

Wang, W., Cheng, W., Duan, J., Gong, J., Hu, B., Angeli, P., 2014. Effect of dispersed holdup on drop size distribution in oil–water dispersions: experimental observations and population balance modeling. Chem. Eng. Sci. 105, 22–31.

Zhou, G., Kresta, S.M., 1998a. Correlation of mean drop size and minimum drop size with the turbulence energy dissipation and the flow in an agitated tank. Chem. Eng. Sci. 53, 2063–2079.

Zhou, G., Kresta, S.M., 1998b. Evolution of drop size distribution in liquid–liquid dispersions for various impellers. Chem. Eng. Sci. 53, 2099–2113.